PHYSICS-BASED MODELLING OF CREEP BEHAVIOUR OF ALUMINIUM ALLOY 2650-T8

A. DJAKOVIC[1], H. C. BASOALTO[2], B. F. DYSON[3] and M. MCLEAN[3]

[1]YU POINT DOO, Francuska 6, 11000 Belgrade, Serbia and Montenegro, a_djakovic@yahoo.com , alex@eph.point-group.com, [2]Qinetiq, Ively Road, Farnborough, Hampshire GU14 0LX, UK, [3]Department of Materials, Imperial College London, Exhibition Road, SW7 2BP, UK

ABSTRACT

A novel continuum damage mechanics model for creep deformation prediction explicitly relating the model parameters to quantitative microstructural measures has been applied for aluminium alloy 2650-T8. A new database of constant-load tensile creep tests has been developed and was used together with data from other sources. The model related the creep response of the alloy to the microstructure that is evolving during creep and successfully described the creep behaviour of the alloy by the concept of damage processes.

Key words: aluminium alloy, 2650-T8, creep, physics-based modelling, continuum damage mechanics, hardening, damage, microstructure evolution, precipitate coarsening, dislocation multiplication, grain boundary cavitation, cavity growth

INTRODUCTION

The creep rupture lifetime solutions of the existing parameteric methodologies are generally found to be unsatisfactory when extrapolating beyond the available dataset. In the case of microstructurally unstable alloys, the Power Law does not offer much advantage due to the continuous variation with stress (and temperature) of the stress exponent constant *n*, the minimum creep rates also being merely a transition between primary and tertiary creep stages and not a steady state. The criticism of some existing empirical fitting models (like the Theta Projection method [1]), which separate the primary and tertiary regimes as independent is in the very assumption that this can be done because the hardening processes responsible for the primary regime and damage mechanisms controlling the creep strain acceleration in the tertiary regime operate simultaneously and interact with each other. The model proposed in this work for aluminium alloy 2650-T8 is based on the existing Physically Based Continuum Damage Mechanics (CDM) model [2-4]. It explicitly considers the microstructural changes and the corresponding micromechanisms occurring during creep, allowing them to interact with each other. It incorporates these in its main constitutive laws and state variables, allowing all microstructural variables to evolve with time. It explicitly relates the model parameters to the quantitative measures of the microstructure, which are hence physically predictive with stress and temperature dependence coming from the real stress and temperature dependence of the microstructural parameters that they consist of.

MODEL FUNDAMENTALS

For precipitate-strengthened alloys, instead of the typical dislocation-dislocation interaction approach, the present model considers dislocation-precipitate interactions to be more appropriate. Traditional approaches to dislocation creep consider the global sequential process of climb and subsequent glide. More realistically, the present model assumes the global behaviour to be a coupled parallel process of climbing dislocations with a small fraction that can at any time glide and contribute the majority of macroscopic creep strain. The creep mechanism is thought to be controlled by the rate at which dislocations become free to glide i.e. escape from the point obstacles, the glide of a free dislocation to the next set of particles being fast. The rate of dislocation escape depends on the stress and temperature for a certain particulate dispersion and the gliding dislocation fraction is not simply geometrical. The hyperbolic sinus (*sinh*) stress function is used to describe the average thermally activated movement of dislocations, biased by the applied stress [2].

Physically Based CDM model is a multi-state variable formulation for creep rates. It incorporates the effects of specific microstructural degradation in a modular manner. It is expressed by a set of coupled non-linear first order differential rate equations for evolution of inelastic strain, internal stress redistribution (hardening) and microstructural damage modes D_i, which are numerically integrated under various boundary conditions, depending on the operating conditions (e.g. constant load/stress creep, variable load/temperature creep etc.). The strain rate is a function of the applied stress σ, temperature T, an evolving hardening parameter H that leads to decelerating strain rate (in primary creep) and the set of evolving damage parameters D_i that lead to accelerating strain rate (in tertiary creep). This model has been presented elsewhere in detail [2-4] as a generic framework applied to many alloy systems.

The main creep strain rate $\dot{\varepsilon}$ equation in the model (flow equation for the matrix creep) not including any damage mechanisms [2-4] is given by Eq. 1:

$$\dot{\varepsilon} = \frac{2\rho_m \quad \phi_p(1-\phi_p)\left[\sqrt{\pi/4\phi_p}-1\right]c_j \quad D_m}{M} \sinh\left(\frac{\sigma_{eff}\,b^2\lambda}{\alpha MKT}\right) \quad \text{or} \quad \dot{\varepsilon} = \dot{\varepsilon}_o \sinh\left(\frac{\sigma}{\sigma_o}\right) \qquad (1)$$

where ρ_m is the mobile dislocation density, ϕ_p the particle volume fraction, c_j the dislocation jog density, D_m the matrix diffusivity, M the Taylor factor, α a constant of the order of unity, b the Burger's vector, λ the interparticle spacing, K the Boltzman constant, T the temperature, $Q_{d/j}$ the combined activation energy for matrix diffusion and jog formation and

$$\sigma_o = \frac{\alpha MKT}{b^2\lambda} \qquad \dot{\varepsilon}_o = \dot{\varepsilon}_o'\exp\left[-\frac{Q_{d/j}}{RT}\right] \qquad D_m = D_{m,o}\exp\left[-\frac{Q_d}{RT}\right] \qquad c_j = c_{j,0}\exp\left[-\frac{Q_j}{RT}\right]$$

$$\dot{\varepsilon}_o' = \frac{2\rho_m\phi_p(1-\phi_p)\left[\sqrt{\pi/4\phi_p}-1\right]c_{j,0}\,D_{m,0}}{M}$$

The effective stress σ_{eff} acting on dislocations is equal to the applied stress σ minus the internal stress σ_i due to stress redistribution around the hard phases (i.e. hardening

mechanism) minus the dislocation network stress σ_d, which is negligible here as the interparticle spacing is smaller than the spacing between dislocations and thus the classical dislocation work-hardening is insignificant. The important model aspect is that the compound parameters $\dot{\varepsilon}_o$ and σ_o consist of microstructural constants and variables and are *entirely predictive* if all necessary material constants are known.

HARDENING MECHANISM

In precipitate-strengthened alloys, the Physically Based CDM model assumes that the hardening mechanism is associated with an internal stress redistribution process from soft plastically deforming regions (α matrix in 2650-T8) to hard non-plastically deforming regions (S'/S particles in 2650-T8) as inelastic strain accumulates in the matrix, thus reducing the effective stress within the matrix ("two-bar" model) [4]. The effective stress in the matrix is hence the difference between the applied stress (σ) and the internal or back stress (σ_i) thrown off the matrix to the particles. The dimensionless hardening parameter H is a measure of this internal back stress and has its evolution law given in Eq. 2:

$$\sigma_{eff} = \sigma - \sigma_i \qquad H = \frac{\sigma_i}{\sigma} \qquad \dot{H} = \frac{h'}{\sigma}\left(1 - \frac{H}{H*}\right)\dot{\varepsilon} \qquad (2)$$

where $h' = \phi_p E_p$ (ϕ_p - particle volume fraction and E_p - particle Young's Modulus) and H* is the maximum value of H (H starts saturating when non-recovery stress relief starts taking place e.g. dislocations cutting through particles, dislocation punch-out, formation of micro-cracks, particle yielding etc.). H* has been given in [2-4] for spherical particles. The author of the present work has modified this formulation for needle-shape S'/S particles, due to the shape strengthening factor [5]. The strengthening coefficient ψ depending on the particle volume fraction ϕ_p and the aspect ratio *L/D* and hence the H* are defined in Eq. 3 as:

$$\psi = 1 + 2(2 + L/D)\phi^{3/2} \qquad H* = 1 - \frac{1}{\psi} \qquad (3)$$

OPERATING DAMAGE MECHANISMS

All damage parameters were defined in a normalised form to vary between zero and unity.

Multiplication of mobile dislocations. The number of dislocations is considered in creep to increase progressively when the stress is applied. Multiplication of mobile dislocations is difficult to investigate as it is hard to distinguish between statistically stored (damage) and geometrically necessary dislocations (required to accommodate inhomogeneous deformation around the hard regions). Dislocation damage parameter D_d and its rate of evolution are defined below in Eq. 4 (where ρ is the dislocation density, i denoting the initial value and C is a material constant):

$$D_d = 1 - \frac{\rho_i}{\rho} \qquad \dot{D}_d = C(1 - D_d)^2\dot{\varepsilon} \qquad (4)$$

Particle coarsening. Components with long service times are usually susceptible to coarsening of a constant volume fraction of strengthening particles. Due to the lifetime

reductions becoming time-dependent at constant temperatures, the influence of the particle coarsening becomes greater at lower stress levels. Assuming a constant particle volume fraction, coarsening damage parameter D_p and its rate of evolution are defined below in Eq. 5 (derived from a standard coarsening equation):

$$D_p = 1 - \frac{r_0}{r} \qquad \dot{D}_p = \frac{k}{3r_0^3}(1 - D_p)^4 \qquad (5)$$

where r is the average effective particle radius at time t (r_0 at t=0) and k is the coarsening rate constant.

Grain boundary cavity growth. Grain boundary creep cavity growth (micromechanism causing low ductility fractures in polycrystalline alloys) was shown in [6] to involve a stress-directed diffusion of atoms from the surface of a cavity to the sinks (sites on a grain boundary). Growth rates slower than the diffusion process have also been reported [7], obeying different mechanics where a structure sensitive deformation process controls the growth instead. Dyson [7-9] introduced the geometrical "constraint" concept as a consequence of an inhomogeneous distribution of cavities. He argued that as the cavities start growing, the two parent grains start moving apart at a rate predicted by the classical diffusive growth, but due to the neighbouring grains being cavity free, the initial unconstrained strain rate is modified according to the way in which the local strain is accommodated. Hence, if the local grain strain rate due to unconstrained cavity growth rate is greater than the creep rate of the neighbouring cavity-free grains (which may be the case at low stress levels), the constrained cavity growth takes place. The necessary compatibility of the overall strain rates of cavitated β and non-cavitated α grains has to be maintained via a stress redistribution process where the cavitated grains throw off some stress onto the neighbouring non-cavitated grains and thus the model has to depict the unconstrained cavity growth at high stress levels, with a transition to the constrained cavity growth as stress level decreases. This is included in Eq. set 6, which is numerically integrated with Eq. 2, 4 and 5 (hardening and other damage modes) using optimised model parameters, for predicting global creep behaviour, individual creep curves and other diagnostic tests.

$$\dot{\varepsilon} = (1 - \phi_c)\dot{\varepsilon}_\alpha + \phi_c(\dot{\varepsilon}_\beta + \dot{\varepsilon}_c)$$

$$\dot{\varepsilon}_\alpha = \frac{\dot{\varepsilon}_0}{(1 - D_{d,\alpha})} sinh\left[\frac{\sigma_\alpha(1 - H_\alpha)}{\sigma_0(1 - D_p)}\right]$$

$$\dot{\varepsilon}_\beta = \frac{\dot{\varepsilon}_0}{(1 - D_{d,\beta})} sinh\left[\frac{\sigma_\beta(1 - H_\beta)}{\sigma_0(1 - D_p)}\right] \qquad (6)$$

$$\dot{\varepsilon}_c = k_c[-2\,ln\,A_c - (1 - A_c)(3 - A_c)]^{-1} \frac{\delta D_{0,b}\,exp(-Q_b/RT)}{T\bar{d}^3\varepsilon_{R,min}^2}(1 - H_\beta)\sigma_\beta$$

$$\dot{\sigma}_\alpha = \frac{\dot{\sigma} - \phi_c\dot{\sigma}_\beta}{1 - \phi_c} \qquad \dot{\sigma}_\beta = E(\dot{\varepsilon} - \dot{\varepsilon}_\beta - \dot{\varepsilon}_c) \qquad \dot{A}_c = \frac{2}{3\varepsilon_{R,min}A_c^{0.5}}\dot{\varepsilon}_c$$

where ϕ_c is the area fraction of cavitated facets in a cross-section; $\bar{d}$ the mean grain size; A_c the evolving area fraction of a cavitated facet and $A_c = (2r_c/\lambda_c)^2$, r_c the cavity radius, λ_c the cavity centre-to-centre spacing; k_c the material specific constant $k_c = 2\pi^3\Omega/9K$, Ω the atomic volume, K the Boltzman's constant; $\delta D_b = \delta D_{0,b}\,exp(-Q_b/RT)$ the grain boundary diffusivity, Q_b the activation energy for grain boundary diffusion; $\varepsilon_{R,min}$ the minimum (lower bound) macroscopic creep ductility, $\varepsilon_{R,min} = \pi\lambda_c/6d$.

TENSILE CREEP OF AS-RECEIVED 2650-T8

Eqs. 1-6 include all measurable microstructural parameters (e.g. average rod precipitate radius, grain size) and also material parameters and state variables that depend on stress and temperature. Hereafter, the creep tests presented are tensile creep tests, unless otherwise stated. Creep data provided by the companies Aerospatiale Matra and Onera (marked as "others") for the ~30μm grain size material (rolling direction) are shown with that from the present work (~40μm).

Global lifetime simulations (stress against time to rupture) are shown in Fig. 1(a), showing that the model simulates very well the available data. The same is true for the global minimum creep rates, Fig. 1(b). In both lifetime and minimum creep rate plots, a transition point between the constrained and unconstrained cavity growth can be noticed i.e. a kink in the plots. Above this kink, the cavity growth is unconstrained and below the kink it is constrained. As explained before, cavitation becomes more important with decreasing stress levels, progressively reducing the lifetime and increasing the minimum creep rates.
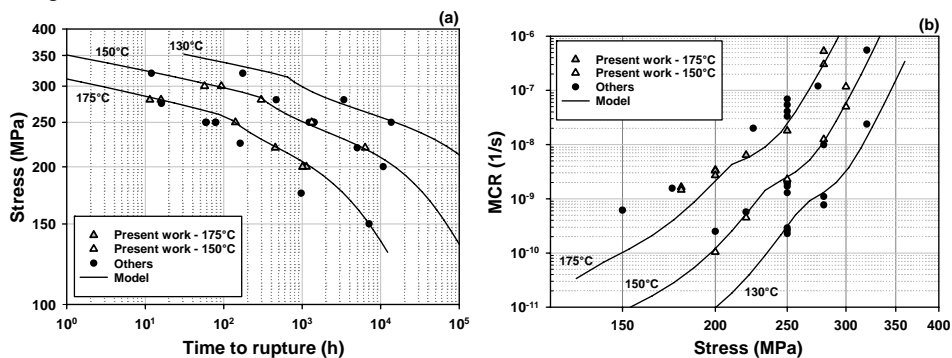

Fig. 1. Comparison between experimental data and model: (a) stress against time to rupture and (b) minimum creep rate against stress
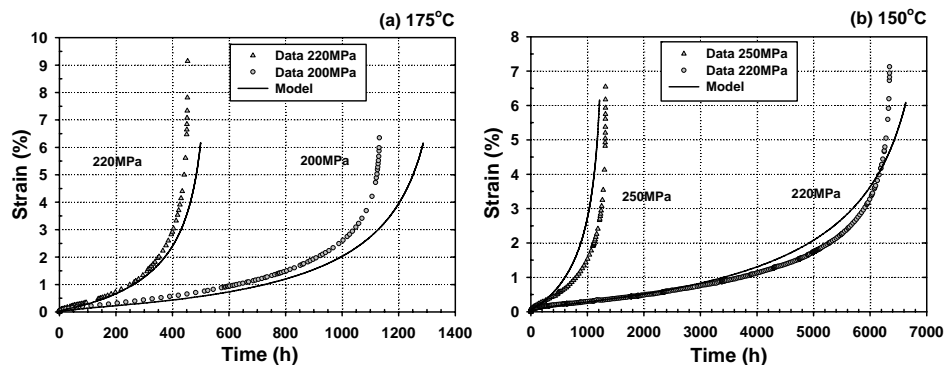

Fig. 2. Experimental data and model creep curves at (a) 175°C and (b) 150°C

Modelling of the individual creep curves and their shapes is demonstrated in Fig. 2 for 175°C and 150°C. It can be concluded that the model predictions agree very well with the creep curves. It should be appreciated that these simulations are not fits to individual creep curves, but are real predictions from the global database. As the

predictions cannot be better than the scatter of the input data, which is large (e.g. lifetime difference of ~40% at 300MPa/150°C), it can be concluded that the physics-based constitutive equations and the operating damage modes appropriately describe the tensile creep behaviour of the alloy.

COMPRESSION CREEP OF AS-RECEIVED 2650-T8

Creep in compression can be used to test for the presence of cavitation damage. Fig. 3(a) shows the tension-compression asymmetry and it also clearly demonstrates that the accelerating tertiary creep regime is present in compression. The difference between the constant load and constant stress predictions is very small (only 15% in lifetime) and cannot account for the asymmetry between the tension and compression, which for the time to 5% strain reaches a 70% difference. The asymmetry is consequently thought to be due to the absence of one damage mode in compression, cavity growth being the only one of the proposed that is dependent upon the stress orientation. The compression model prediction for 250MPa and 175°C is also shown in Fig. 3(a). Identical equations and parameters were used both in tension and compression, the only difference being the cavitation that is disregarded in compression, with a "negative" constant load effect. It can be seen that the model can predict the large asymmetry in time to a particular strain.
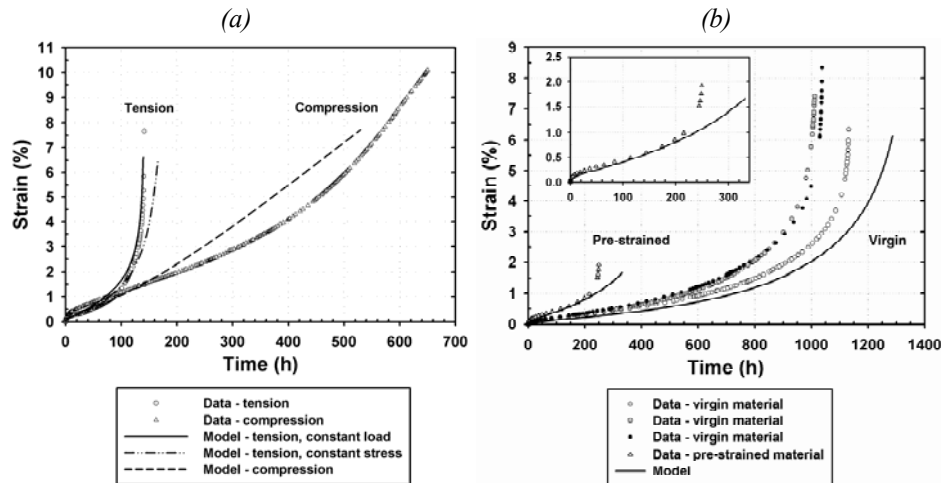

Fig. 3. Data and model comparison for (a) tension and compression at 250MPa and 175°C; (b) as-received material and 4.9% plastically pre-strained, crept at 200MPa and 175°C

CREEP OF THE PRE-STRAINED 2650-T8

Creep comparison of the as-received material and the 4.9% plastically pre-strained is shown in Fig. 3(b) (200MPa and 175°C). Identical equations are used for both virgin and pre-strained materials and only two parameters were changed: $\varepsilon_{R,min}$ was decreased from 6.5% to 2% (experimental observation) and $\dot{\varepsilon}_o'$ was calculated to increase from 2.8×10^8 s^{-1} to 9.8×10^8 s^{-1} due to the increased mobile dislocation density (prior plastic deformation).

It can be concluded from Fig. 3(b) that the model predicts very well the creep curve of the pre-strained sample, larger overall creep rates and much shorter lifetime and

rupture strain, and that the concept of grain boundary cavitation as defined in the model appears to offer a suitable description of the grain boundary damage. The final parts of tertiary regime predictions are not as steep as the data, probably due to necking (even for the pre-strained sample, some signs of necking were found).

CREEP OF OVERAGED 2650-T8

The as-received alloy was overaged 2,000h at 182°C and tested in creep. These results are compared to those of the as-received material in Fig. 4. Precipitate particles have grown during overageing and the average initial precipitate rod radius r_0 has increased from 4nm to 7.14nm, as measured. σ_o was also changed because it is affected by the changes in the interparticle spacing. Since λ was not calculated for the overaged material, reduction in σ_o was made on the basis of 12.4% reduction in the hardness value and by assuming $H_v \propto 1/\lambda$. Due to the very high rupture strains of the overaged material (twice as high as in the virgin material), cavitation was excluded for the overaged material. It can be seen from Fig. 4 that the model lifetime prediction agrees well with the data for the overaged material.
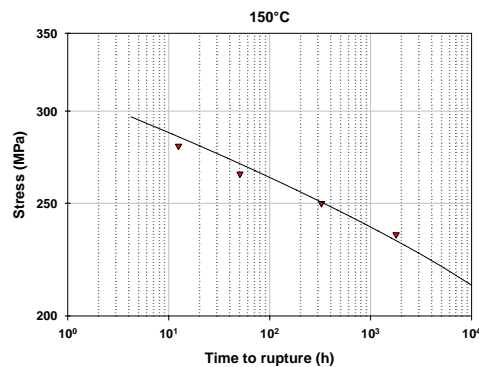

Fig. 4. Creep of material overaged 2,000h at 182°C: data and model lifetime comparison

STEP LOADING TEST

Changing the loading conditions can severely affect the alloy creep performance due to the change in underlying damage mechanisms. Any non-physically based model is destined to be very misleading in variable loading conditions. In this work, only one creep step-test was performed: initial step involved creep at 200MPa and 150°C for 8,974h generating ~0.41% creep strain and in the second step only the loading was changed to 280MPa.

Fig. 5 shows that damage accumulated during the first 8,974h loading at 200MPa giving only ~0.41% accumulated strain substantially shortened the lifetime for the second step at 280MPa and 150°C (~ ½ an order of magnitude). The model agrees well with the data in both the first and the second step. Special emphasis must be placed here on the fact that the model predicts exceptionally well the shape of the curve in the second step and in the apparent second primary creep stage right after the stress increase. The apparent second primary is due to the further stress transfer being possible as a result of the increased applied load. The Strain Hardening model (also shown here)

grossly overestimates the step-test lifetime, especially overestimating the second step duration by a factor of ~4 and not predicting the correct curve shape, entirely missing out the second primary stage. Hence, the model proposed in this work is superior due to its physics based origin. It includes the correct microstructural mechanisms, appropriate state variables and their evolution laws.
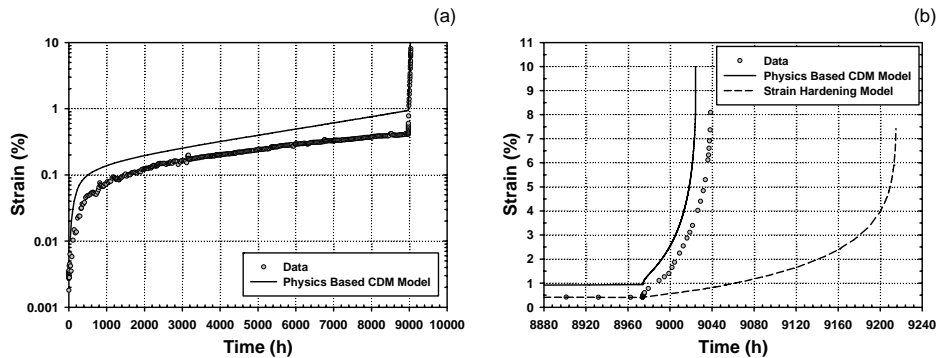

Fig. 5. Creep step-test: comparison between the data and (a) the predictions of the Physics Based CDM model and (b) the Strain Hardening model

CONCLUSIONS

The Physically Based Continuum Damage Mechanics model proposed in this work predicts very well the lifetimes, minimum creep rates, creep curves and their shapes in the aluminium alloy 2650-T8. It explicitly considers the microstructural changes and the corresponding micromechanisms during creep, explicitly relating the model parameters to the quantitative measures of the microstructure and allowing for the interaction of different damage modes through the creep strain rate equation. For a full global description, three damage modes are necessary: dislocation multiplication, grain boundary cavity growth and precipitate coarsening. Omitting one can be extremely misleading as the dominant damage mode could change with the changing operating conditions. Pre-strained and compressive creep tests and a step-test confirmed the correct choice of damage modes for the alloy.

The model output can identify the regimes of damage mode dominance, and this can be very useful for alloy design and development. Due to the physics-based links with the microstructure, the proposed model can be used to investigate the effects of the changes in the precipitate or dislocations structures, grain size etc. on the creep behaviour.

ACKNOWLEDGMENTS

REFERENCES

[1] R.W. Evans and B. Wilshire, in *Structural Materials: Engineering Application Through Scientific Insight*, edited by E.D.Hondros and M.McLean (1996), Institute of Materials, London, pp.155-172.

[2] B.F.Dyson and M.McLean, Microstructural Stability of Creep Resistant Alloys for High Temperature Plant Applications (number 2), edited by A.Strang, J.Cawley and G.W.Greenwood, The Institute of Materials, London (1998), pp.371-393.

[3] B.F.Dyson, *Use of CDM in Materials Modelling and Component Creep Life Prediction*, J. Pressure Vessel Technology, Trans. ASME (2000), 122 (No.3), pp.281-296.

[4] B.F.Dyson, in *Creep Deformation: Fundamentals and Applications*, edited by R.S.Mishra, J.C.Earthman and S.V.Raj, pp.309-318, proceedings of 2002 TMS Annual Meeting and Exhibition, Seattle, Washington, February 17-21, 2002.

[5] J.Rosler, G.Bao and A.G.Evans, Acta Metall. Mater. 39 number 11 (1991), pp.2733-2738.

[6] R.K.Varma and B.F.Dyson, Scripta Metall. 16 (1982) pp. 1279-1284.

[7] B.F.Dyson, *Constrained Cavity Growth: Its Use in Quantifying Recent Creep Fracture Results*, Canadian Metallurgical Quarterly 18 (1979) pp. 31-38.

[8] B.F.Dyson, in *Creep and Fracture of Engineering Materials and Structures*, edited by B.Wilshire and D.R.J.Owen, Pineridge Press (1981) pp. 235-247.

[9] B.F.Dyson, Metal Science 10 (1976) pp. 349-353.